Available online at www.sciencedirect.com
SCIENCE DIRECT
Polymer 45 (2004) 8367–8375
polymer
www.elsevier.com/locate/polymer

# Aliphatic poly(oxytetramethylene) ionenes: effect of counter-anion on the properties and morphology

Yuko Ikeda*, Jyunya Yamato, Takeshi Murakami[1], Kanji Kajiwara[2]

*Faculty of Engineering and Design, Kyoto Institute of Technology, Matsugasaki, Sakyo, Kyoto 606-8585, Japan*

Received 11 June 2004; received in revised form 3 September 2004; accepted 30 September 2004
Available online 22 October 2004

**Abstract**

Effect of counter-anion on the properties and morphology of aliphatic poly(oxytetramethylene) ionenes was investigated, and the relationship between the properties and morphology was elucidated. The ionenes possess elastic properties at low elongations whereas they predominantly exhibit a plastic deformation at high elongations. The morphology of the ionenes was analysed in the nanometer scale by fitting a cascade model for randomly branched *f*-functional polycondensates incorporated in Debye–Bueche random-two-phase model and the interference term by the interdomain interaction on their small-angle X-ray scattering profiles. The size of ionic domains and distance between the domains were smaller and shorter in the ionene with bromide counter-anion than those in the ionene with chloride counter-anion, respectively. The formation of crystallite of poly(oxytetramethylene) (POTM) segments was detected in the ionene with chloride counter-anion at room temperature. These characteristics of aliphatic POTM ionenes gave the difference in their mechanical and thermal properties.


*Keywords:* Ionene; Morphology; Properties

## 1. Introduction

A new type of physical networks like a thermoplastic elastomer has been developed and widely used as an elastomer with high performance and high function [1]. The physically aggregated phases, such as glass phase and crystalline phase, of physical networks cooperatively function as quasi crosslinking sites and fillers, when they are microphase-separated from the amorphous matrix. In the case of ionomers, the ionic segments aggregate in the polymer matrix to induce the microphase separation, which can also result in the network formation. Since the properties of physically crosslinked elastomers depend on their spatial morphologies in general, it is necessary to study the relationship between the properties and morphology in detail.

There are several useful methods available to investigate the morphology of polymers such as a transmission electron microscopy (TEM), atomic force microscopy (AFM) and X-ray scattering [2–7]. These methods have been developed significantly in the last decade. The microscopy gives us a direct imaging of the morphology to the angstrom scale and often supports the results of morphological analysis by other techniques. In the field of X-ray scattering, on the other hand, a recent progress of synchrotron radiation has expanded the study on the polymer morphology. For example, a small-angle X-ray scattering (SAXS) by a synchrotron radiation is capable to quickly and dynamically reveal the spatial correlation in the scattering system on a scale from 10 to 1000 Å. These methods are complementarily utilised for the morphological study in polymer science.

To date, many studies on the morphology of physically crosslinked elastomers by SAXS have been reported [2–7]. Recently, we have carried out the SAXS measurements to investigate the morphology of several physically crosslinked elastomers which we made [8–11], on the basis of

* Corresponding author. Tel.: +81 75 724 7558; fax: +81 75 724 7580.
*E-mail address:* yuko@ipc.kit.ac.jp (Y. Ikeda).
[1] Present address: Polymer Technology Laboratory, NSK Ltd., Kugenuma, Shinmei, Fujisawa 251-8501, Japan.
[2] Present address: Faculty of Home Economics, Ohtuma Women's University, Sanban-cho, Chiyoda-ku, Tokyo 102-8357, Japan.

0032-3861/$ - see front matter © 2004 Elsevier Ltd. All rights reserved.
doi:10.1016/j.polymer.2004.09.082

a cascade model for randomly branched *f*-functional polycondensates incorporated in the Debye–Bueche random-two-phase model and the interference term by the interdomain interaction [12–17]. The new model assumed a most probable spatial distribution of crosslinking domains in the morphology of physically crosslinked elastomers [8–11], which was consisting of the amorphous matrix and the aggregated domains. Here, the domains constituted quasi crosslinks and were distributed over the amorphous polymer matrix in such a way that the space correlation was described by a tree-like network. The repulsive interaction was also considered to exist between the domains. This new model could successfully account for the wide range of SAXS profile of our physically crosslinked elastomers, including the upturn of the scattering intensity toward zero angle, little full interpretation on which has been provided. Namely, the cascade model for gel formation was found to give the smart explanation for the sharp upturn of the scattering intensity toward zero-angle of physically crosslinked elastomers. Especially, this analytical method was useful for the samples, whose morphology was difficult to be appeared by microscopic observations.

In this paper, the effect of counter-anion on the morphologies of aliphatic poly(oxytetramethylene) ionenes (IP) is investigated and the relationship between the morphologies and properties is elucidated on the basis of our proposed model described above. The chemical structure of IPs is illustrated in Fig. 1. The samples with $Cl^-$ and $Br^-$ are abbreviated as IP-Cl and IP-Br, respectively Since a living poly(oxytetramethylene) (POTM) can be reacted with nucleophiles to give various kinds of macromolecules such as amphiphilic and ionic linear polymers, star polymers, graft polymers and networks, the many studies on the ring-opening polymerization of tetrahydrofuran (THF) and characterization of the obtained macromolecules have been reported [8–11, 18–33]. However, the relationship between the properties and morphology of POTM ionenes has not been well understood, although the ionenes showed excellent mechanical properties. Thus, it will be emphasised in this article that the counter-anion of aliphatic POTM ionenes influences their morphology and consequently their properties, by using the results of differential scanning calorimetry (DSC), SAXS, wide-angle X-ray diffraction (WAXD), dynamic mechanical analysis (DMA) and tensile measurement.

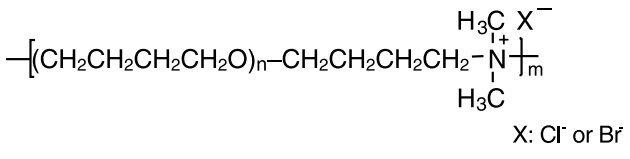


Fig. 1. Chemical structure of IP-Cl and IP-Br.

## 2. Experimental

### 2.1. Materials

Aliphatic POTM ionenes with chloride anions and bromide anions were synthesised by cationic living polymerization of THF using $(CF_3SO_2)_2O$ (0.23 mol/l) as an initiator at 0 °C under dry nitrogen atmosphere for 5 min, followed by chain-extension reaction by adding six times amounts of *N*,*N*′-dimethylaminotrimethylsilane relative to the concentration of the initiator at 0 °C [33]. The yield was 16%. The exchanges of counter-anion of the ionene from $CF_3SO_3^-$ to halide anions were conducted by pouring the THF/methanol (1/1) mixed solution of the polymer to 0.5N-sodium chloride or 0.5N-sodium bromide aqueous solutions at room temperature (r.t.), respectively, and the procedure was repeated four times. The polymers were purified by the precipitation method from the methanol solution to water and followed by dialysis in water for ca. 30 h using Cellulose Dialyzer Tubing VT351 (Nacalai Tesque, Inc., Japan, cut-off 3500). This procedure was repeated three times and the polymers were dried at 30 °C under the reduced pressure.

The chemical structures of IP-Cl and IP-Br were confirmed by $^1$H-NMR and $^{13}$C-NMR on a Fourier-transform high resolution NMR spectrometer JEOL GX-400 (Nippon Denshi Co.) in $CDCl_3$ with tetramethylsilane at r.t. IP-Cl: $^1$H-NMR; $\delta$: 1.62 ppm (methylene protons of –$CH_2CH_2CH_2CH_2O$–), $\delta$: 3.41 ppm (methylene protons of –$CH_2CH_2CH_2CH_2O$–), $\delta$: 3.33 ppm (methyl protons of –$N^+(CH_3)_2$–). $^{13}$C-NMR; $\delta$: 26.24, 26.43, 26.62, 26.67 ppm (methylene carbons of –$CH_2CH_2CH_2CH_2O$–), $\delta$: 70.21, 70.30, 70.41, 70.50, 70.61 ppm (methylene carbons of –$CH_2CH_2CH_2CH_2O$–), $\delta$: 69.19 ppm (methylene carbons of –$OCH_2CH_2CH_2CH_2$–$N^+(CH_3)_2$–), $\delta$: 29.61 ppm (methylene carbons of –$OCH_2CH_2CH_2CH_2$–$N^+(CH_3)_2$–), $\delta$: 19.97 ppm (methylene carbons of –$OCH_2CH_2CH_2CH_2$–$N^+(CH_3)_2$–), $\delta$: 63.59 ppm (methylene carbons of –$OCH_2CH_2CH_2CH_2$–$N^+(CH_3)_2$–), $\delta$: 50.96 ppm (methyl carbons of –$N^+(CH_3)_2$–). IP-Br: $^1$H-NMR; $\delta$: 1.62 ppm (methylene protons of –$CH_2CH_2CH_2CH_2O$–), $\delta$: 3.41 ppm (methylene protons of –$CH_2CH_2CH_2CH_2O$–), $\delta$: 3.33 ppm (methyl protons of –$N^+(CH_3)_2$–).

IR measurement of the ionenes was also carried out on an infrared spectrometer FTIR-4100 (Shimadzu Co.). IR (thin films prepared by casting from the chloroform solutions at 30 °C): IP-Cl: $\nu(CH_2)$ 2855, 2938 $cm^{-1}$, $\nu$(C–O–C) 1113 $cm^{-1}$, $\delta$(CH) 1368 $cm^{-1}$. IP-Br: $\nu(CH_2)$ 2859, 2938 $cm^{-1}$, $\nu$(C–O–C) 1111 $cm^{-1}$, $\delta$(CH) 1368 $cm^{-1}$.

Molecular weight between the ionic units was measured by a quantitative analysis using an inversion recovery method in $^1$H-NMR. IP-Cl: 2380, IP-Br: 2480. The molecular weights between the ionic units were also evaluated by an elemental analysis. IP-Cl: 2340, IP-Br: 2250. Both values were almost in good agreement for IP-Cl and IP-Br, respectively. The elemental analysis of the

ionenes was conducted at the Elemental Analysis Center of Kyoto University. IP-Cl. Anal. Calcd C; 65.87, H; 11.14, N; 0.59, Cl; 1.49. Found: C; 63.66, H; 11.25, N; 0.59 Cl; 1.34. IP-Br. Anal. Calcd C; 64.76, H; 10.92, N; 0.60, Br; 3.42. Found: C; 63.27, H; 11.27, N; 0.60 Br; 2.93. From the data of nitrogen contents, the degrees of exchange reaction of counter-anion for IP-Cl and IP-Br were estimated to be 90 and 86%, respectively.

The reduced viscosity ($\eta_{sp}/c$) of the ionenes was measured with an Ubbelohde viscometer at 30 °C in a thermostatic bath. The ionenes were dissolved in 0.1N methanol solution of ammonium chloride and ammonium bromide for IP-Cl and IP-Br, respectively. $\eta_{sp}/c$ is plotted as a function of concentration ($c$) and the intrinsic viscosity was determined. Here, $\eta_{sp} = (\eta - \eta_0)/\eta_0$, where $\eta$ and $\eta_0$ represent the viscosity of the solution and solvent, respectively. The intrinsic viscosity of IP-Cl and IP-Br were 0.58 and 0.55 dl/g, respectively. In our previous paper, the weight average molecular weight ($M_w$) of IP-Br, whose intrinsic viscosity was 0.44 dl/g in 0.1N methanol solution of ammonium bromide at 30 °C, was measured to be 48,000 g/mol by a light scattering measurement [33]. Although the $M_w$ of IP-Cl and IP-Br studied here was not measured, it was estimated to be larger than 48,000 g/mol.

### 2.2. Preparation of IP-Cl and IP-Br films

The films of IP-Cl and IP-Br were prepared by casting their 5% chloroform solutions on Teflon molds at 30 °C and were dried under a reduced pressure at 30 °C. The thickness of the films was ca. 1 mm. The sample films were subjected to the measurements after annealing at 40 °C for 12 h under vacuum and followed by standing for one day under dry atmosphere.

### 2.3. Differential scanning calorimetry

DSC measurement was carried out on a Rigaku Thermoflex DSC-8230 under nitrogen. The sweep rate of temperature was 10 °C/min. The sample loaded was ca. 10 mg.

### 2.4. Dynamic mechanical analysis

The temperature dispersions of dynamic shear modulus ($G'$) and loss tangent ($\tan\delta$) of the polymer film were measured on a dynamic mechanical analyzer (DVE-4V Rheospectra of Rheology Co., Ltd., Japan). The sample dimension was 5 mm × 5 mm × ca. 1 mm. The strain mode was used and the heating rate was 2 °C/min. The frequency was 10 Hz.

### 2.5. Tensile measurement

Tensile test was carried out using a Tensile Tester TOM 100D (Shinko Tsushin Kogyo Co. Ltd.) on ring-shaped dry samples at 25 °C. The extension speed was set to be 100 mm/min.

### 2.6. Small-angle X-ray scattering measurement

SAXS measurement was carried out with the SAXES optics installed at BL-10C of the Photon Factory, Tsukuba, Japan [34], where an incident X-ray from synchrotron was monochromatised to the wavelength of the X-ray ($\lambda$) = 1.488 Å with a double-crystal monochrometer and focused to the cell position with a bent focusing mirror. The scattered X-ray was detected by the one-dimensional position sensitive proportional counter of an effective length 160 mm positioned at the distance of about 1.0 m from the sample holder. The SAXS intensities were accumulated for an appropriate period of time to attain a sufficient S/N ratio. The exact camera distance was calibrated by using the diffraction peaks of the collagen fiber (the long period = 670 Å) at the sixth, ninth and eleventh orders. Data were collected on a CAMAC system controlled by a NEC PC 9801 RX. The scattered intensities were corrected with respect to the variation of the incident X-ray flux by monitoring the beam with an ionizing chamber placed in front of the thermostated sample folder.

### 2.7. Wide-angle X-ray diffraction analysis

WAXD measurement was carried out at r.t. using a rotating-anode X-ray generator (Rigaku–Denki, RU-300) operated at 40 kV and 240 mA. Cu Kα X-ray beams monochromatised with a graphite monochrometer were shone onto the specimen through a pinhole collimator of 0.5 mm in diameter. As an X-ray detector, the IP system (MAC Science, DIP-220) was utilised.

## 3. Basic formulation

Gelation in general has been described in terms of multifunctional reaction in the classic Flory–Stockmayer (FS) model [35]. Although many models were proposed to improve our understanding on gelation mechanism, the FS model has an advantage in its simplicity to specify the gelling system explicitly with two parameters (i.e., the functionality ($f$) and the fraction of reacted functional groups $\alpha$) and defines a gel point uniquely. The model was also applied to calculate the scattering profile from the gelling system within the framework of the cascade process [16,17,36–38].

The cascade theory for random $f$-functional polycondensates [12] was extended to calculate the scattering intensity as a function of the magnitude of the scattering vector ($q$) for the gelling system [13,14]. Since the scattering intensity ($I(q)$) was given for the system where the scattering units were dispersed as [39]

$$I(q) = \sum_{i=1}^{n}\sum_{j=1}^{n} A_i A_j \sin(qr_{ij})/q_{ij} \quad (1)$$

when $A_i$ denoted the scattering amplitude of the $i$th scattering unit, and $r_{ij}$ was the distance between the $i$th and $j$th units.

The scattering intensity from random $f$-functional polycondensates was calculated from Eq. (1) as [40]

$$I(q) = A^2(q)(1 + a\varphi)/[1 - (f-1)\alpha\Phi] \quad (2)$$

$$\Phi \equiv \exp(-b^2q^2/6) \quad (3)$$

Here $\alpha$ was the fraction of reacted functional groups, and $b^2$ was the mean-square distance between two nearest units. The magnitude of the scattering vector was defined in term of the wavelength of an incident beam ($\lambda$) and the scattering angle ($\theta$) as

$$q = (4\pi/\lambda)\sin(\theta/2) \quad (4)$$

Eq. (2) involved three parameters, $\alpha$, $f$ and $b$. However, in reality $(f-1)\alpha \leq 1$ up to the gel point and $\Phi < 1$, so that $\alpha\Phi \ll 1$. In these conditions, Eq. (2) was determined by two parameters,$b$ and $(f-1)\alpha$.

Eq. (2) implied that the scattering amplitude was assumed to be common for all scattering units distributed randomly in the system, so that $A^2(q)$ corresponded to the particle scattering factor of the scattering unit. $A^2(q) = 1$ for a point-like scattering unit as originally derived [36]. The divergence of the scattering intensity at $q \to 0$ was expected upon gelation from Eq. (2), which was also confirmed experimentally.

In the case of physically crosslinked elastomers, the model is considered to be composed of the small heterogeneous domains, which are distributed over the space (polymer matrix) in a random fashion, specified by the cascade process [8]. The small heterogeneous domains constitute the quasi crosslinks, which correspond to the scattering units in the model. Since random association forms the heterogeneous domains, the segment distribution in the domains is supposed to be represented by the Debye–Bueche correlation function. Thus, Eq. (2) is rewritten for the model of the heterogeneous domains forming the cascade network as

$$I(q) \approx I_{\mathrm{D-B}}(q)(1 + \alpha\Phi)/[1 - (f-1)\alpha\Phi] \quad (5)$$

Here $f$ denotes the average number of ties from a single heterogeneous domain. $b^2$ in Eq. (5) corresponds to the mean-square distance between the nearest-neighbour heterogeneous domains. When the interdomain interaction is taken into account, Eq. (5) is further modified as

$$I(q) \approx [I_{\mathrm{D-B}}(q)(1 + \alpha\Phi)/[1 - (f-1)\alpha\Phi]]S(q) \quad (6)$$

where $S(q)$ denotes the interference term caused by the interdomain interaction.

The interdomain interaction is represented by the repulsion between domains. Since the heterogeneous domains undergo thermal motion in the rubbery state, the interaction is averaged over the distribution of domain sizes and thermal motion. Thus, the interdomain interaction potential could be represented by a Gaussian type, and consequently the interference term is written as

$$S(q) \approx 1/[1 - C\exp(-\xi^2q^2)] \quad (7)$$

where $\xi$ is the correlation length specifying the range of interaction, and $C$ is a constant depending on the concentration, the second virial coefficient and the weight average molecular weight.

## 4. Results and discussion

### 4.1. Mechanical properties of IP-Cl and IP-Br

Fig. 2 shows the stress–strain curves of IP-Cl and IP-Br films. Both films displayed very small stresses at low elongations and rises of stress at high elongations. The residual strain of these ionenes became large with the increase of strain. For example, the residual strain after 100% stretching was very small, whereas that after 300% stretching was ca. 20%. Since the stress of these ionenes was increased by a strain-induced crystallization of POTM segments, the residual strain became large at high elongations due to the plastic deformation of POTM crystalline phases of the ionenes. Generally, physically crosslinked elastomers such as a thermoplastic elastomer show both elastic and plastic deformations during stretching. Therefore, IP-Cl and IP-Br were classified as a physically crosslinked elastomers. Comparing the tensile properties of the samples, the abrupt increase of stress up to ca. 30 MPa was observed at ca. 800% elongation for IP-Br film, which suggests that the stress-induced crystallization of POTM segments of IP-Br was more significantly

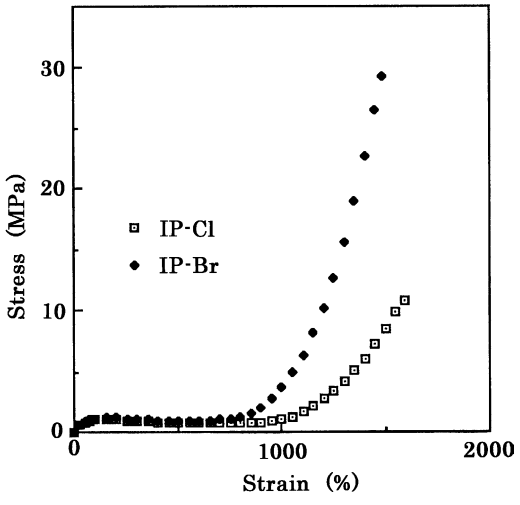


Fig. 2. Stress–strain curves of IP-Cl and IP-Br at 25 °C.

promoted than that of IP-Cl. The different characteristics of these films were also appeared in their dynamic mechanical properties.

Fig. 3 shows the temperature dispersions of $G'$ of these ionene films. In both samples, the drops of $G'$ ascribed to the glass transition of amorphous POTM phase, the melting of POTM crystalline phase and the dissociation of ionic aggregates were clearly detected during heating from −120 °C. However, the $G'$ of IP-Br above the glass transition was larger than that of IP-Cl, and the flatter rubbery plateau region was clearly observed in the former than in the latter. Additionally, the physically aggregated ionic domains of IP-Br, which function as crosslinking sites, were more stable against the dynamic motion of DMA under heating than those of IP-Cl. These differences suggest that the morphologies of IP-Cl and IP-Br were not same. Since their molecular weights between the ionic units and intrinsic viscosities of IP-Cl and IP-Br were similar, respectively, the difference in the chemical structures between IP-Cl and IP-Br is considered to influence their mechanical properties. Namely, a kind of counter-anion of the ionenes is predicted to affect the formation of their higher-order structures, which gave the characteristic feature on their mechanical properties shown in Figs. 2 and 3.

### 4.2. Thermal properties of IP-Cl and IP-Br

The distinct feature of these ionenes was also detected in

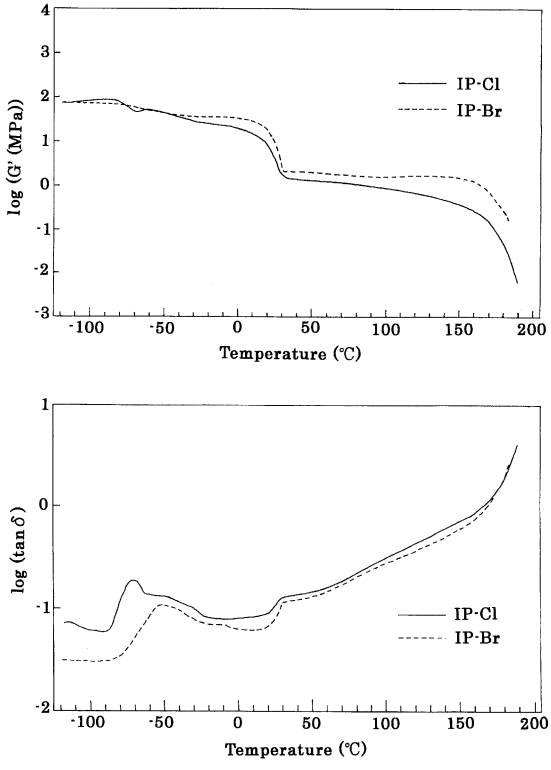


Fig. 3. Temperature dispersions of $G'$ and tan $\delta$ for IP-Cl and IP-Br.

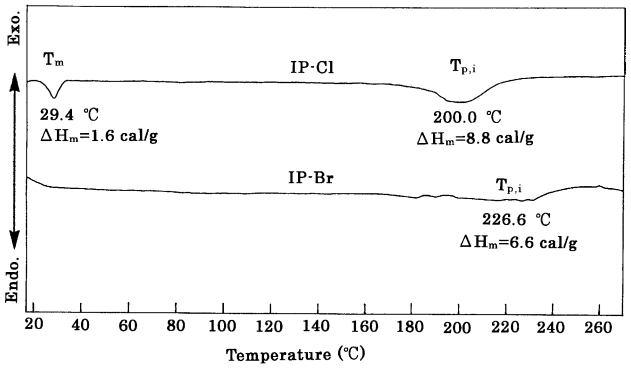


Fig. 4. DSC curves of IP-Cl and IP-Br measured from r.t. to 270 °C.

thermal properties. Figs. 4 and 5 show the DSC curves of the sample films. The former displays the results of heating process from r.t. to 270 °C and the latter does those of cycle measurement from −120 to 150 °C. As shown in Fig. 4, the melting peak of POTM crystalline phase was not detected in IP-Br during heating from r.t., whereas it was clearly appeared at 29.4 °C for IP-Cl. Additionally, the phase transition temperature of the dissociation of ionic segment domains ($T_{p,i}$) was found to be higher and broader in IP-Br than in IP-Cl. These observations suggest that the ionic segments of the former aggregated more tightly and stably than those of the latter. Consequently, the ionic domains

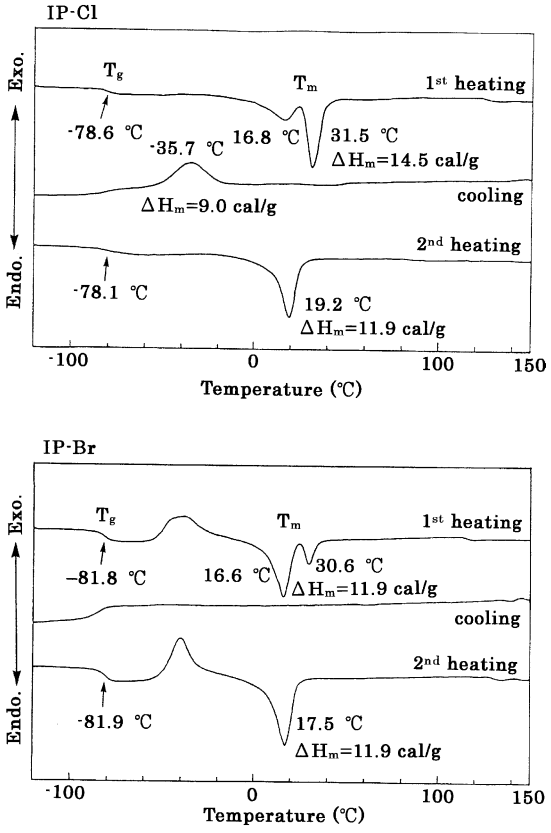


Fig. 5. DSC curves of IP-Cl and IP-Br measured repeatedly from −120 to 150 °C.

seem to have prevented the crystallization of POTM segments in IP-Br at r.t. The difference in the thermal stability of ionic domains for the samples was in good agreement with those detected by DMA.

These thermal characteristics of the ionenes also appeared in the cycle measurement of DSC. As shown in Fig. 5, the amorphous POTM phase of IP-Br was recrystallised at ca. −20 °C during first heating of 10 °C/min, whereas that was not detected in IP-Cl. It was attributable to the presence of much amorphous phase in IP-Br at r.t., which was also resulted in lower $T_g$, lower $T_m$ and smaller heat of fusion in the melting ($\Delta T_m$) of IP-Br than those of IP-Cl. In the rapid cooling process by pouring liquid nitrogen by hand, the amorphous POTM of IP-Br was hardly crystallised due to the presences of ionic domains, and followed by recrystallising the POTM amorphous phase during heating at 10 °C/min. Therefore, the melting peak at 16.6 °C is ascribed to the melting of newly formed POTM crystalline phase by recrystallisation.

On the other hand, the recrystallisation process was not detected for IP-Br in the cooling process from 150 °C, whereas the clear recrystallisation peak was appeared at −35.7 °C in the DSC curve of IP-Cl under the cooling from 150 °C. This difference suggests that the presence of ionic domains in the IP-Br matrix prevented the recrystallisation of POTM segments under cooling condition of this study. These results also suggest the difference in the higher-order structures of these ionenes, especially in the formations of ionic domains and crystalline phases in the matrixes.

### 4.3. Morphology of IP-Cl and IP-Br

The results of DMA, DSC and tensile test indistinctly give us the image of morphologies for IP-Cl and IP-Br, but the detail on their morphology such a size of ionic domain and distance between the ionic domains in the POTM matrix was not clear. Additionally, our TEM and AFM were not useful for these samples to observe their morphologies. Thus, the films of IP-Cl and IP-Br were subjected to the SAXS measurement for their morphological study, and the obtained SAXS profiles were analysed by our proposed method for physically crosslinked elastomers [8–11].

In Fig. 6, the observed SAXS profiles at r.t. from IP-Cl and IP-Br are illustrated, where one broad scattering peak was appeared in each film. This means that there existed no well-ordered morphology, such as lamellae, hexagonally close-packed cylinders and simple cubic packed spheres, which can be identified from the relative peak positions in the SAXS profile. Then, each profile from the ionenes was analysed using Eq. (6), that is, in term of the cascade model incorporated in the Debye–Bueche term and the interaction term, according to the method of our previous reports [8–11]. As shown in this figure, good fittings were achieved in all $q$ regions between the observed SAXS data and calculated scattering profiles based on Eq. (6). Here, the model is described by a set of structural parameters; the size

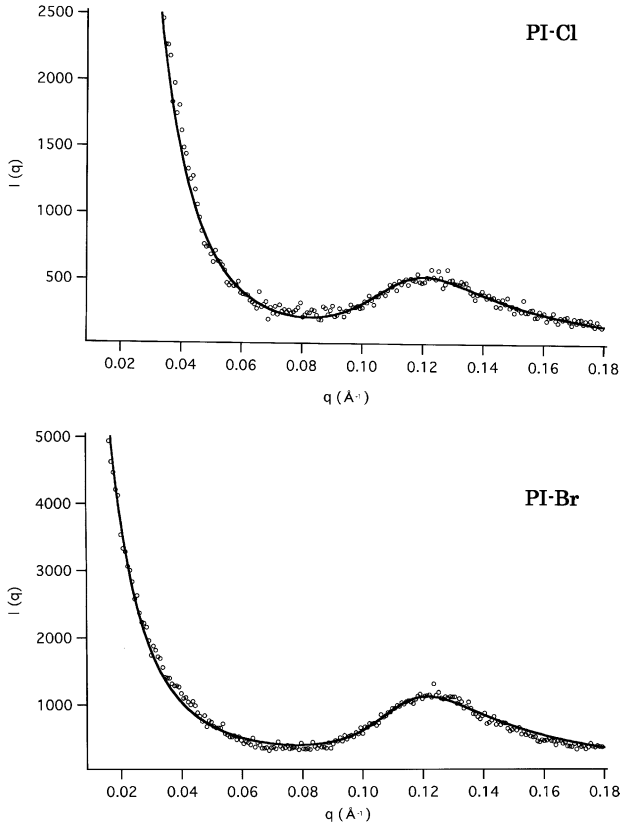


Fig. 6. Observed SAXS profiles (○) of IP-Cl and IP-Br at 25 °C and the calculated profiles based on Eq. (6) (solid lines).

of the physically aggregated ionic domains ($a$), the average distance between the centers of neighbouring aggregated ionic domains ($b$) and their interaction distance ($\xi$). Table 1 summarises the values of structural parameters, which yielded the best fitting profiles to respective observed SAXS data. Here, the product of $\alpha$ and $(f-1)$ was found to be almost 1 in both samples, which means that these ionenes were in the vicinity of the gel point at r.t. from the viewpoint of the cascade model. Schematically, the morphologies of IP-Cl and IP-Br are displayed in Fig. 7 using these structural parameters shown in Table 1 and the results of DSC. The higher-ordered structure of IP-Br was concluded to be composed of the amorphous POTM segments matrix and ionic segments domains, whereas that of IP-Cl was composed of three phases, i.e., the amorphous POTM segments matrix, POTM crystalline phase and ionic segments domains.

The presence of crystallites in IP-Cl was supported by WAXD measurements as shown in Fig. 8, where a diffraction ring and amorphous hallow were detected at

Table 1
Structural parameters determined by SAXS at 25 °C

| Sample code | $a$ (Å) | $b$ (Å) | $\xi$ (Å) | $(f-1)\alpha$ |
|---|---|---|---|---|
| IP-Cl | 21.0 | 61.3 | 23.4 | 1.00 |
| IP-Br | 15.4 | 54.7 | 24.8 | 0.96 |

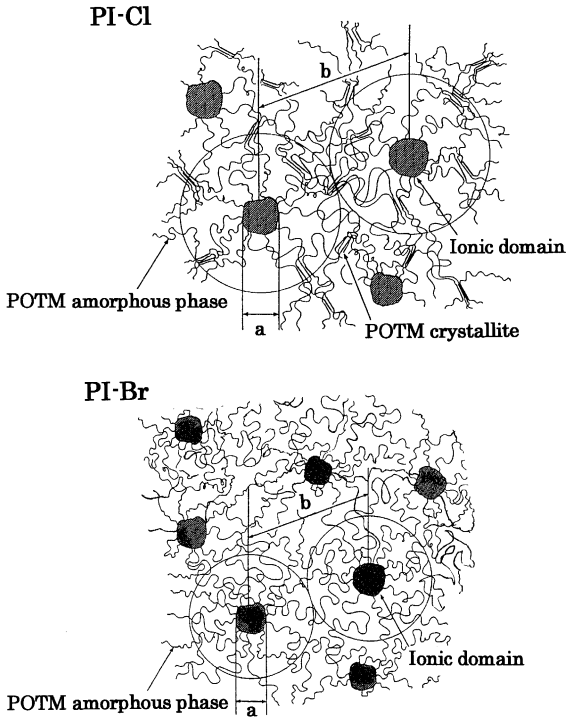


Fig. 7. Schematic morphologies of IP-Cl and IP-Br at 25 °C.

r.t. However, the diffraction ring was not so clear, which means the crystalline phase of PI-Cl was not so stacked. Since no scattering peak due to the POTM crystalline phase was also detected in SAXS at r.t. for IP-Cl, the crystalline phase of IP-Cl is considered to be composed of POTM crystallites. The WAXD of IP-Br, on the other hand, showed only amorphous hallow at r.t. These observations were also in good agreement with the DSC results.

### *4.4. Relationship between the properties and morphology of aliphatic POTM ionenes*

The SAXS analysis based on the cascade model for randomly branched *f*-functional polycondensates incorporated in the Debye–Bueche random-two-phase model and the interference term by the interdomain interaction brought about useful results to discuss the relationship between the properties and morphology of the ionenes. Namely, the smaller size of ionic domain and shorter distance between the ionic domains in IP-Br than in IP-Cl at r.t. were clearly appeared in the nanometer scale as shown in Table 1. These observations mean that the crosslinking density of IP-Br was larger than that of IP-Cl. The smaller ionic domains dispersed in IP-Br matrix with a higher crosslinking density in the amorphous POTM matrix compared with IP-Cl, which gave characteristics of mechanical properties to IP-Br film: the $G'$ above 30 °C was larger, the rubbery plateau regions were flatter and the stress at r.t. was higher in IP-Br than in IP-Cl, although the POTM crystallites existed in IP-Cl at r.t.

In this SAXS analysis, the correlation length of interaction between the ionic domains ($\xi$) was also evaluated. Since the $\xi$ should in principle serve as a measure for the distance over which the interaction between domains extends, the mechanical properties of the aliphatic POTM ionenes may be related with this contribution. The $\xi$ of both ionenes was similar with each other, but the difference between the value of $2\times\xi$ and $b$ was smaller in IP-Br than in IP-Cl. This may suggest that the interaction between the ionic domains of IP-Br was stronger than that of IP-Cl, which brought about the high performance on the mechanical properties for IP-Br.

Naturally, the properties of ionenes are also significantly influenced by the degree of microphase separation between the ionic segments and POTM segments. From the results of DSC and DMA, the good microphase separation between the ionic segments and POTM segments was qualitatively detected in both IP-Cl and IP-Br. Since the $T_g$ and tan $\delta$ peak corresponding to the $T_g$ of IP-Br were lower and shaper than those of IP-Cl, respectively, the microphase separation of IP-Br seems to occur more clearly than IP-Cl. This point

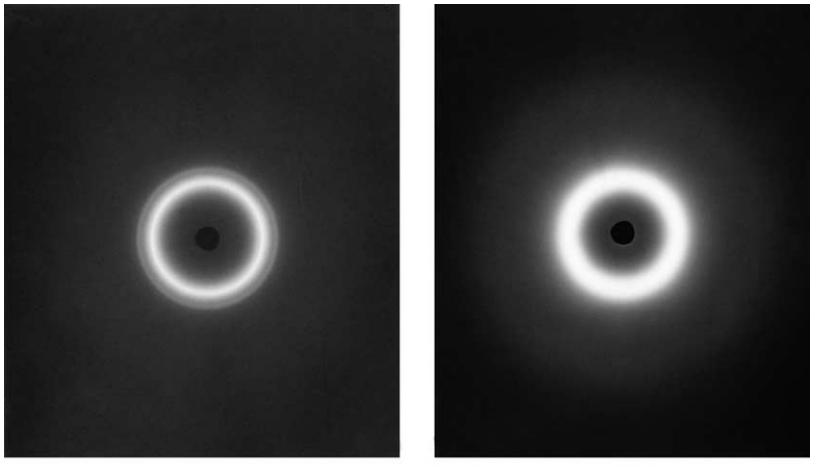


Fig. 8. WAXD patterns of IP-Cl and IP-Br at r.t.

may be one of the reasons for IP-Br to show the better mechanical properties than IP-Cl.

It is worth noting that the stress-induced crystallization of POTM segments was promoted in IP-Br. The morphology of these ionenes during stretching should be significantly changed. Thus, we will investigate their morphology under stretching in near future.

## 5. Conclusions

Aliphatic POTM ionenes with chloride anions and bromide anions were synthesised, and the effect of counter-anion on their properties and morphology was investigated by tensile measurement, DSC, DMA, WAXD and SAXS. The ionenes were classified as physically crosslinked elastomers. The nano-scale structure of ionenes was appeared by SAXS using a cascade model for randomly branched *f*-functional polycondensates incorporated in Debye–Bueche random-two-phase model and the interference term by the interdomain interaction. The smaller size of ionic domain and shorter distance between the ionic domains in IP-Br than in IP-Cl at r.t. gave characteristics of mechanical properties to IP-Br film: the $G'$ above r.t. was larger, the rubbery plateau regions were flatter and the stress at r.t. was higher in IP-Br than in IP-Cl. The analytical method based on the cascade theory for physically crosslinked elastomers is concluded to be one of the powerful techniques for evaluation of the morphology of ionic elastomers, especially when a direct observation by TEM and AMF cannot be conducted. The morphological change of the ionenes during stretching is our next subject and will be reported in elsewhere.

## Acknowledgements

We thank Prof. Dr. S. Kohjiya of Kyoto University for his valuable discussions. This research was partially supported by Grant-in-Aid for Science Research on Priority Area (B) No.740/11229202 and on Priority Area (A) No.413/14045247 from the Japanese Ministry of Education, Science, Sports and Culture.

## References

[1] Holden G, Legge NR, Quirk R, Schroder HE, editors. Thermoplastic elastomers. 2nd ed. Munchen: Hanser; 1996.
[2] Grady BP, Cooper SL. In: Mark JE, Erman B, Eirich FR, editors. Science and technology of rubber. 2nd ed. San Diego: Academic Press; 1994 (chapter 13).
[3] MacKnight WJ, Lundberg RD. In: Holden G, Legge NR, Quirk R, Schroder HE, editors. Thermoplastic elastomers. 2nd ed. Munchen: Hanser; 1996 (chapter 10B).
[4] Hashimoto T. In: Holden G, Legge NR, Quirk R, Schroder HE, editors. Thermoplastic elastomers. 2nd ed. Munchen: Hanser; 1996 (chapter 15A).
[5] Hoseman R, Baguchi SN. Direct analysis of diffraction by matter. Amsterdam: North-Holland; 1962.
[6] Tant MR, Wilkes GL. J Macromol Sci, Rev Macromol Chem Phys 1988;C28(1):1.
[7] Maurtz KA. J Macromol Sci, Rev Macromol Chem Phys 1988; C28(1):65.
[8] Ikeda Y, Murakami T, Yuguchi Y, Kajiwara K. Macromolecules 1998;31:1246.
[9] Ikeda Y, Murakami T, Kajiwara K. J Macromol Sci-Phys 2001;B40: 171.
[10] Ikeda Y, Yuguchi Y, Kajiwara K, Murakami T, Kohjiya S. Presented at German Rubber Conference 2000, Nurnberg, Abstract; 2000. p. 199.
[11] Ikeda, Y. Presented at the136rd Spring Technical Meeting, Rubber Division, ACS; 2003. Paper no. 10.
[12] Gordon M. Proc Roy Soc (London) 1961;A268:240.
[13] Kajiwara K, Burchard W, Gordon M. Br Polym J 1970;2:110.
[14] Kajiwara K. J Chem Phys 1971;54:296.
[15] Debye P, Bueche AM. J Appl Phys 1949;20:518.
[16] Urakawa H, Ikeda Y, Yuguchi Y, Kajiwara K, Hirata Y, Kohjiya S. In: Osada Y, Khokhlov AR, editors. Polymer gels and networks. New York: Marcel Dekker; 2001 (chapter 1).
[17] Urakawa H, Yuguchi Y, Ikeda Y, Kajiwara K, Hirata Y, Kohjiya S. In: Bohidar HB, Dubin P, Osada Y, editors. Polymer gels fundamentals and applications. Washington, DC: ACS; 2002. p. 70.
[18] Smith S, Hubin AJ. J Macromol Sci Chem 1973;A7:1399.
[19] Goethals EJ, editor. Telechelic polymers: synthesis and applications. Boca Raton, FL: CRC Press; 1989.
[20] Goethals EJ, Caeter PV, Geeraert JM, Du Prez FE. Angew Makromol Chem 1994;223:1.
[21] Kohjiya S, Ohtuki T, Yamashita S. Makromol Chem Rapid Commun 1981;2:417.
[22] Kohjiya S, Hashimoto T, Yamashita S, Irie M. Chem Lett 1985;1497.
[23] Kohjiya S, Hashimoto T, Yamashta S. Makromol Chem Rapid Commun 1989;10:9.
[24] Kohjiya S, Ikeda Y, Moriya N, Hahimoto T, Yamashta S, Shibata Y. MRS Int Mtg Adv Mater 1989;12:255.
[25] Kohjiya S, Ohtuki T, Yamashita S. Makromol Chem 1990;191:397.
[26] Kohjiya S, Ohtuki T, Yamashita S, Taniguchi M, Hashimoto T. Bull Chem Soc Jpn 1990;63:2089.
[27] Hashimoto T, Kohjiya S, Yamashita S, Irie M. J Polym Sci Part A; Polym Chem Ed 1991;29:651.
[28] Kohjiya S, Hashimoto T, Yamashita S. J Appl Polym Sci 1992;44: 555.
[29] Tezuka Y, Shida T, Shiomi T, Imai K. Macromolecules 1993;26:575.
[30] Hashimoto T, Sakurai S, Morimoto M, Nomura S, Kohjiya S, Kodaira T. Polymer 1994;35:2672.
[31] Murakami T, Ikeda Y. Koubnnshi Ronbunsyu 1998;55:637.
[32] Murakami T, Ikeda Y, Urakawa H, Kajiwara K, Kohjiya S. Rubber Chem Technol 2000;73:864.
[33] Ikeda Y, Murakami T, Urakawa H, Kohjiya S, Grottenmuller R, Schmidt M. Polymer 2002;43:3483.
[34] Ueki T, Hiragi Y, Izumi Y, Tagawa H, Kataoka M, Muroga M, Matsushita T, Amemiya Y. Photon Factory Rep 1983;IV:70.
[35] See, for example, Flory PJ. Principles of polymer chemistry. Ithaca, NY: Cornell University Press; 1953.
[36] Kajiwara K, Kohjiya S, Shibayama M, Urakawa H. In: Rossi DeD, Kajiwara K, Osada Y, Yamaguchi A, editors. Polymer gels. New York: Plenum; 1991. p. 3.
[37] Yuguchi Y, Mimura M, Urakawa H, Kajiwara K. In: Stokke BT, Elgsaeter A, editors. Polymer networks group review series, vol. 2. New York: Wiley; 1999. p. 343.
[38] Yamanaka S, Yuguchi Y, Urakawa H, Kajiwara K, Kohjiya S. Network Polym, Jpn 1999;20:157.

[39] Debye P. In: McIntyre D, Gornick F, editors. Light scattering from dilute polymer solutions. New York: Gordon & Breach; 1964.
[40] Eq. (2) was introduced from Eq. (1) based on the concept and vocabulary of graph theory, which provided the combinatorics of branched polymer systems. The intensity of scattering based on the cascade model was found to be described using the $z$-average particle scattering factor $Pz(\theta)$ of polymer distributions. See the detail in Refs. [13,14].